The porous $ZnCo_2O_4$ nanosheets arrays as a binder-free electrode for high performance flexible supercapacitor materials

Jing Wang (wangwangmayong@126.com)
harbin university of commerce https://orcid.org/0000-0002-2459-2683
Chen Wang
Harbin University of Commerce
Shen Wang
Harbin Institute of Technology
Xiang Zhang
Harbin Institute of Technology
Xiangyang Jin
Harbin University of Commerce
Jiang Chang
Harbin University of Commerce
Jing Dong
Harbin University of Commerce

Research Article

Keywords: ZnCo2O4 nanosheets arrays, Flexible electrode, Asymmetric supercapacitors device, High energy density

Posted Date: March 4th, 2021

DOI: https://doi.org/10.21203/rs.3.rs-271126/v1

Abstract

In this paper, the porous $ZnCo_2O_4$ nanosheets arrays (NAs)/carbon cloth (CC) were prepared for the first time as a binder-free anode by hydrothermal method. The anode electrode material shows multistage pore distribution and thus can provide numerous ways for the transport of ions and electrons. As a supercapacitor electrode, the flexible $ZnCo_2O_4$/CC electrode indicates a high specific capacitance (1790 F/g at the current density of 1 A/g), good rate performance, and excellent cycle properties (99.4% capacitance retention after 10000 cycles). Besides, the flexible electrode also displays good mechanical flexibility. The solid-state asymmetric flexible supercapacitor device was assembled taking the $ZnCo_2O_4$/CC electrode as the positive electrode and carbon nanotube (CNTs)/CC as the negative electrode. The asymmetric device delivers high energy density 47.1 Wh/Kg (power density 800 W/Kg) and power density 12000 W/Kg (energy density 28.3 Wh/Kg) with the potential window 0 V ~ 1.6 V. These results indicate the $ZnCo_2O_4$/CC flexible electrode with high electrochemical performance adjust for environmentally friendly and low-cost energy storage devices in the future.

1. Introduction

With the rapid development of flexible/bendable electronic device, flexible energy storage devices have attracted wide attention. Supercapacitors (SCs) are deemed to be one of the flexible energy storage devices due to the excellent electrical advantages such as long cycles, fast charge-discharge ability, high power density, and so on [1–4]. But the insufficient energy density of SCs restrict their further application in daily life. The energy density is related to specific capacitance (C) and potential window (V) based on $E = 1/2CV^2$ [5–9]. For improving the energy density, the asymmetric supercapacitors device should be assembled by integrating different electrode material. Meanwhile, the device will show a wide range of voltage window (~ 2 V) in aqueous electrolytes[10–15]. Hence, the preparation of high-performance electrode material with outstanding mechanical performance is an effective strategy to fabricate an excellent flexible SC.

In recent years, binary metal oxides exhibit better pseudocapcitor electrochemical properties than the single component metal oxides because of their higher electronic conductivity, higher theoretical capacity and reversible redox reactions [16–21]. Among the various binary metal oxides, $ZnCo_2O_4$ materials as active materials for supercapacitors are reported promising electrode materials due to their better electrochemical performance, higher conductivity, low cost and environmental friendliness [22, 23]. Such as, Patil et al. prepared $ZnCo_2O_4$ microstrips/carbon cloth and displays the good cycling performance 94% capacitive retention over 1000 cycles in 1 M KOH aqueous electrolyte [24]. Liu and his coworkers synthesized three-dimensional $ZnCo_2O_4$ nanowire arrays/carbon cloth anode for Li-ion battery with high reversible capacitance of 1300–1400 mAh g^{-1} [25]. Wu et al. prepared $ZnCo_2O_4$ nanorods arrays/carbon cloth and the $ZnCo_2O_4$-CC//PPy-CC asymmetric supercapacitor exhibits an energy density of 2.3 mW h /cm^2 at a power density of 18.9 mW h/cm^3 [26]. Therefore, a simple and mild route to construct high-

perforce $ZnCo_2O_4$ flexible electrode is important to realize the practical application of flexible energy storage electronic devices.

In this paper, we prepare the porous $ZnCo_2O_4$ nanosheets arrays grown directly on the surface of the flexible carbon cloth using one-step simple hydrothermal method with heat treatment. These nanosheets with porous structure connected with each other form numerous holes, which are contributed to the electrolyte ion and electrons transportation among the interface and surface of the materials. The electrochemical tests indicate the binder-free electrode shows high specific capacitance of 1790 F/g at the current density of 1 A/g, rate property of 68%, cycling performance with the capacitance retention 99.4%. The asymmetric supercapacitors are assembled taking the porous $ZnCo_2O_4$ nanosheets arrays as the positive and the carbon nanotubes as the negative. The device displays a wide potential window of 1.6 V, high energy density of 47.1 Wh/kg (at the power density of 800 W/kg) and excellent cycling performance.

2. Experiments

In the experiments, the reagents were used with analytical grade and did not further purification. Carbon cloth (1 x 1 x 0.1 cm^3) was used as conductive collector and cleaned by sonication method in the 6 M HNO_3, ethanol and deionized water about 1 h, respectively.

2.1 The preparation of the porous $ZnCo_2O_4$ NAs/CC electrode

The porous $ZnCo_2O_4$ NAs were prepared directly grown on carbon cloth by one pot hydrothermal method. Firstly, 0.8 mmol Zn $(NO_3)_2$•$6H_2O$, 2.5 mmol $Co(NO_3)_2$•$6H_2O$, 3 mmol $CO(NH_2)_2$ and 1.5 mmol NH_4F were mixed in 30 ml of deionized water with sonication for 3.5 h. The above mixtures were transferred into a 50 ml Teflon-lined stainless-steel autoclave with a piece of cleaned carbon cloth. The autoclave was sealed and maintained at 150 ℃ for 6 h. Then the samples were cooled down to the room temperature, taken out and cleaned with ethanol and the deionized water for three times and dried at 50 ℃ for 8 h, followed by annealing at 550℃ in air for 5 h so that obtained the porous $ZnCo_2O_4$ NAs/CC electrode (~ 1 cm^2 area; $ZnCo_2O_4$ NAs mass: 2.1 mg).

2.2 The preparation of carbon nanotubes (CNTs)/CC electrode

The CNTs/CC electrode was prepared as followed: firstly, taking 0.5 g CNTs and dropped 60 ml 80 % HNO_3, then heated the mixture at 80 ℃ for 18 h followed by constant stirring. When the mixtures cooled down to room temperature, cleaned the CNTs with ethanol and deionized water for three times, respectively and dried at 50 ℃ for 10 h. The CNTs/CC electrode was prepared by mixing CNTs (80 wt %), carbon black (10 wt %) and polyvinylidenefluoride (PVDF, 10 wt %). A small amount of ethanol was then

added to the above mixtures. Taking the mixtures coated onto the surface of CC and dried at 90 ℃ for 6 h.

2.3 The preparation of the gel-state asymmetric supercapacitors

The asymmetric supercapacitors device was assembled by using $ZnCo_2O_4$/CC electrode as positive and CNTs/CC electrode as negative with a separator. PVA/KOH was used as the gel-state electrolyte. PVA/KOH gel electrolyte was synthesized by mixing KOH 2.8 g and PVA 3 g into 25 ml deionized water, then heated at 80℃ and stirred for 5 h. The two electrodes and the separator were soaked in PVA/KOH gel electrolyte for a few minutes. Then taken them out from the gel and assembled together. The device was placed in air for 12 h and became solid state. The electrochemical properties of the device were tested by an electrochemical CHI 660E workstation, made in Shanghai, China. The electrochemical tests of the as-prepared electrodes were firstly performed in a three-electrode system with 2 M KOH as electrolyte. Pt plate was used as the counter electrode and the saturated calomel electrode (SCE) was used as the reference electrode. Cyclic voltammetry (CV), Galvanostatic charge-discharge (GCD) and electrochemical impedance spectroscopy (EIS, 0.01–100 kHz with an amplitude of 5 mV) were firstly tested in a three-electrode cell, the capacitance was calculated as follows:

$$C_m = I\Delta t / m\Delta V \quad (1)$$

C_m ($F \cdot g^{-1}$) is the specific capacitance of a single electrode. I (A) represents the current of discharge and Δt(s) is the discharge time. m(g) is the mass of the active material and ΔV (V) is the potential window.

The electrochemical measurements of the device of the energy density (E) and power density(P) were calculated from the following equation:

$$E = 1/2CV^2 \quad (2)$$

$$P = E/\Delta t(s) \quad (3)$$

2.4. Materials characterization

The morphology of the as prepared samples were examined by scanning electron microscopy (SEM, JEOL JSM-7500F) and transmission electron microscopy (TEM, JEOL JEM-2100F). The crystal structures of the as-prepared materials were observed by X-ray diffraction (XRD, RigakuD/max-2600 PC) with the Cu Karadiation (1.5406Å). The electrochemical tests were performed by a Shanghai Chenhua CHI660E electrochemical workstation.

3. Results And Discussion

The morphology of the as-prepared samples were tested by SEM. Figure 1a shows the carbon cloth with the diameter 15 um for a single carbon fiber. After a simple one-step hydrothermal process with heat

treatment, the as-prepared $ZnCo_2O_4$ NAs with high density are uniformly grown on the surface of the carbon fibers as shown in Fig. 1b. The magnified image of Fig. 1c indicates a large number of $ZnCo_2O_4$ NAs grown on the carbon fiber. Figure 1d further confirmed $ZnCo_2O_4$ NAs have the thickness of 10 nm and these nanosheets connected with each other forming porous structures. Further taking the hole section of Fig. 1d for SEM mapping, the results indicate the existence of Zn, Co, O and C elements as shown in Fig. 1e. Figure 1f shows the corresponding EDS tests, indicating the Zn, Co, O and C elements can be found. These results are consistent with the Fig. 1e SEM mapping tests.

The microstructures of the as-prepared products were further detected by TEM tests. From the Fig. 2a, these nanosheets are some porous structures and these nanosheets arrays connected with each other forming holes can be found. The mesoporous properties of the thin nanosheets are generally attributed to the re-crystallization reaction and the liberation of gas during the thermal treatments. Figure 2b demonstrates the lattice spacing of 0.23 nm and 0.24 nm, corresponding to the (222) and (311) lattice planes of $ZnCo_2O_4$. The inset in Fig. 2b shows the corresponding selected area electron diffraction (SAED) patterns, indicating the polycrystalline properties of the as-prepared samples. Taking the section of Fig. 2a for TEM mapping is shown in Fig. 2c, Zn, Co, O and C elements still can be found. The results are consistent with the SEM mapping tests and EDS tests. The crystal structures of $ZnCo_2O_4$ were detected by X-ray diffraction (XRD) tests in Fig. 2d, which confirm the $ZnCo_2O_4$ (JCPDS Card No. 23-1390). This porous $ZnCo_2O_4$ nanosheets strucure was further researched by BET (Brunauer-Emmett-Teller) N_2 adsorption desorption tests. The results were shown in Fig. 3 with the specific surface area 116.86 $m^2\ g^{-1}$. This porous configuration is mainly due to the porous structure of $ZnCo_2O_4$ and the interconnected $ZnCo_2O_4$ nanosheets grown directly on the carbon cloth nanofibers scaffold. The special nanosheets structures display not only large specific surface area, high electrolyte permeability, but also allow fast ion and electron transportation.

The electrochemical performances of the $ZnCo_2O_4$ NAs/CC are firstly tested in a three-electrode system with 2M KOH as the electrolyte to study the potential application of the flexible electrode. The CV curves of carbon cloth (CC) and $ZnCo_2O_4$ NAs/CC at the scan rate of 5 mV/s is shown in Fig. 4a. The results demonstrated that the porous $ZnCo_2O_4$ NAs/CC electrode shows higher capacitive performances than the pure carbon cloth, and reveal the pure carbon cloth contributes little to the capacitance of the porous $ZnCo_2O_4$ NAs/CC electrode. Figure 4b exhibits the charge-discharge curves of carbon cloth and $ZnCo_2O_4$ NAs/CC electrode at the current density of 3 A/g. The discharge time of $ZnCo_2O_4$ NAs/CC electrode is longer than carbon cloth. According to Eq. 1, the specific capacitance of carbon cloth and $ZnCo_2O_4$ NAs/CC electrode are calculated at the same current density of 3A/g and are shown in Fig. 4c. The results further confirm the carbon cloth (30 F/g) shows little performance to the total capacitance of $ZnCo_2O_4$ NAs/CC electrode (1560 F/g). Figure 4d exhibits the CV curves of $ZnCo_2O_4$ NAs/CC electrode at different scan rates of from 10 to 100 mV/s. The CV curves indicate the pseudocapacitance properties of $ZnCo_2O_4$ NAs and the curves remains basically the same at the scan rate increases, demonstrating the good reversibility. When the scan rate increase, the peak current increase indicating the fast electron and ionic

transportation of the as prepared $ZnCo_2O_4$ NAs/CC electrode. Charge-discharge curves were also tested at different current densities of 1, 2, 5, 10, 15 and 20 A/g in Fig. 4e. These charge-discharge curves with good symmetry revealed the desirable electrochemical reversibility. The specific capacitances of the $ZnCo_2O_4$ NAs/CC electrode were calculated are 1790, 1620, 1450, 1360, 1290 and 1120 F/g at the current density of 1, 2, 5, 10, 15 and 20 A/g, respectively, as shown in Fig. 4f. The porous $ZnCo_2O_4$ NSs/CC electrode with a high specific capacitance at the current density of 1 A/g is higher than the hexagonal $ZnCo_2O_4$ electrode (846 F/g) [23], core-shell $ZnCo_2O_4$@$NiCo_2O_4$ structures (1476 F/g) [27], and the porous $ZnCo_2O_4$ hollow spheres (1150 F/g) [28]. And the specific capacitance of 1120 F/g at high current density of 20 A/g is also higher than the core-shell $ZnCo_2O_4$@$NiCo_2O_4$ electrode (942 F/g) [27], mesoporous $ZnCo_2O_4$ microspheres (830 F/g) [29], the carbon nanofiber@$ZnCo_2O_4$ (940 F/g) [30], and the $ZnCo_2O_4$/ZnO@multiwall carbon nanotube (1705 F/g) [31]. These results show the good capacitive activities of the as-prepared porous $ZnCo_2O_4$ NSs/CC electrode. A cycling test was examined at the current density 2 A/g for 10000 cycles as shown in Fig. 4g. The specific capacitance of $ZnCo_2O_4$ NAs/CC electrode changes from 1620 F/g to 1610 F/g, which keeps the capacitance retention of 99.4%. The SEM and TEM images of electrode after 10000 cycles have been provided as shown in Fig. 5 and Fig. 6. The results indicate the materials have good structural stability, and the morphology keep consistent after 10000 cycles. We compare our work with the as reported specific capacitances and cycling performance of the reported other binary oxides. $ZnCo_2O_4$ based electrodes and the present work is shown in Table 1.

Table 1
Comparison of specific capacitances and cycling performance of the reported other binary oxides, $ZnCo_2O_4$ based electrodes and the present work.

Electrode materials	Current density	Capacitance (F/g)	Cycles	Retention	Ref
$ZnCo_2O_4$ nanorod	2 mA/cm^2	305	3500	92%	[32]
$NiMoO_4$ Nanosheet	5 A/g	847.7	10000	89.2 %	[33]
$CoMoO_4$-$NiMoO_4 \cdot xH_2O$ bundles	2.5 mA/cm^2	1039	1000	72.3 %	[34]
$NiMoO_4$ nanoflake	5 mA/cm^2	131.8	6000	94.2%	[35]
$ZnCo_2O_4$ microspheres	1 A/g	647.1	2000	91.5 %	[36]
$NiMoO_4$/$CoMoO_4$ nanorods	1 A/g	1445	3000	78.8%	[37]
$NiCo_2O_4$@$NiMoO_4$	2 mA/cm^2	1389	2000	90.6%	[38]
$ZnCo_2O_4$/ZnO	5 A/g	304	5000	68.7%	[39]
peony-like $ZnCo_2O_4$	1 A/g	440	3000	67.7%	[40]
$ZnCo_2O_4$ NAs/CC	2 A/g 3.6 mA/cm^2	1620	10000	99.4 %	This work

Figure 4h shows the last 10th cycle tests of charge-discharge curves. The charge-discharge curves are consistent without obvious changes, indicating good cycle properties. The Nyquist plots of the $ZnCo_2O_4$ NAs/CC electrode after 1st and 10000th cycles are detected in Fig. 4i. The arc increments are no obvious difference indicating the structures well maintained with 10000 cycles. The slope of the curve is the Warburg impedance increased after 10000 cycles, attributing to the loss of a few active materials during the charge and discharge process. Rate and cycle performance of the hybrid $ZnCo_2O_4$ NAs/CC electrode under different current densities as shown in Fig. 7. Changing the current density at different forms and returning to the original forms, the specific capacitance basically unchanged. Figure 8a shows the image of the as prepared $ZnCo_2O_4$ NAs/CC electrode with the size 1 x 1 cm^2. The CV curves in four twisting and bending forms (Fig. 8b) are shown in Fig. 8c. The results confirm the $ZnCo_2O_4$ NAs/CC electrode has good mechanical stability.

In order to further explore the potential application of the as-prepared electrode, an asymmetric supercapacitor (ASC) device was assembled by CNTs/CC as the negative and $ZnCo_2O_4$ NAs/CC as the positive. Figure 9 shows the CV curves of the $ZnCo_2O_4$ NAs/CC electrode and CNTs/CC electrode

performed in a three-electrode cell in 2 M KOH electrolyte at a scan rate of 15 mV/s. Figure 10 shows the charge and discharge curves of the CNTs. The charge and the mass ratio between the negative and the positive are calculated according to the specific capacitance and potential windows range. Figure 11a exhibits the illustration of the ACS device. Figure 11b shows the CV curves of the $ZnCo_2O_4$ NAs/CC//CNTs/CC device at different potential windows. The ACS device can make the potential range for 1.8 V. But the CV curve at 0-1.8 V was unstable due to the hydrogen evolution. The results indicate the stable potential window range is 0 ~ 1.6 V. Figure 11c shows the CV curves of the ACS device at different scan rates. The CV curves remain the same shape during the scan rate increased, indicating a good stability and fast transportation property of ions and electron. Charge-discharge tests of the ACS device were explored at different current densities of 1, 2, 5, 8, 10 and 15 A/g is illustrated in Fig. 11d. The charge/discharge curves were nearly symmetrical, suggesting good electrochemical stability and capability. The specific capacitance of the device was calculated from the discharge curves and the results is shown in Fig. 11e. The specific capacitances of the device are 131, 106, 94, 85,75 and 70 F/g at the current density of 1, 2, 5, 8,10 and 15 A/g, respectively. The Ragone plots of the ACS device were recorded in Fig. 11f. The device with high energy density and power density were calculated according to the Eqs. 2 and 3. The maximum energy density 47.1 Wh/kg is obtained at a current density of 1 A/g and the corresponding power density is 800 W/kg under the operating voltage of 1.6 V. This device possesses a maximum power density 12000 W/kg at the current density of 15 A/g and the energy density is 28.3 Wh/kg with the same potential window 1.6 V. Finally, we compared this work with the reported work as shown in Fig. 5f [41–46].

4. Conclusion

In summary, the porous $ZnCo_2O_4$ NAs were successfully prepared by one-stephydrothermal method and succedent thermal treatment. The porous $ZnCo_2O_4$ NAs/CC electrode shows a high specific capacitance 1790 F/g at the current density of 1/A g and good cycle performance of 94% capacitance retention at the current density of 2 A/g after 10000 cycles. The $ZnCo_2O_4$ NAs/CC//CNTs/CC ASC device demonstrates high energy density 47.1 Wh/kg (at the power density of 800 W/kg) and power density 12000 W/kg (at the energy density of 28.3 Wh/kg), these results confirm the as-prepared electrode and device will be promising energy storage device in the future.

Declarations

Credit authorship contribution statement

Jing Wang designed this experiment, carried out the electrochemical experiments, wrote the the manuscript and other analysis. Chen Wang and Shen Wang carried out the characterization tests, analyzed, wrote the results and revised the manuscript. Jiang Chang and Xiangyang Jin analyzed the characterization tests, wrote and revised the manuscript. Chen Wang and Jiang Chang analyzed and discussed the results.

Acknowledgments

This research work was supported by the National Natural Science Foundation of China (No.52002099), young scientists foundation from Harbin University of Commerce, China (2019CX28) and the Young scientific research item of Harbin University of Commerce, Heilongjiang province, China (No.2019DS084).

Declaration of interests

The authors declare that they have no known competing financial interests or personal relationships that could have appeared to influence the work reported in this paper.

References

1. B. Dunn, H. Kamath, J.M. Tarascon, Science. **334**, 928–935 (2011)
2. Q. Liu, X. Hong, X. Zhang, W. Wang, W. Guo, X. Liu, M. Ye, Chem. Eng. J. **356**, 985–993 (2019)
3. L.R. Hou, Y.Y. Shi, C. Wu, Y.R. Zhang, Y.Z. Ma, X. Sun, J.F. Sun, X.G. Zhang, C.Z. Yuan, Adv. Funct. Mater. **28**, 1705921 (2018)
4. *A.M. Zardkhoshoui*, *S.S.H. Davarani*, Dalton T. 49, 10028–10041(2020)
5. H. Liang, C. Xia, A.H. Emwas, D.H. Anjum, X. Miao, H.N. Alshareef, Nano Energy. **49**, 155–162 (2018)
6. T. Xiong, T.L. Tan, L. Lu, W.S.V. Lee, J. Xue, Adv. Electron. Mater. **8**, 1702630 (2018)
7. Y. Zhu, Q. Zong, Q. Zhang, H. Yang, Q. Wang, H. Wang, Electrochim. Acta **299**, 441–450 (2019)
8. T. Chen, S. Li, P. Gui, J. Wen, X. Fu, G. Fang, Nanotechnology. **29**, 205401 (2018)
9. *R. Arian*, *A.M. Zardkhoshoui*, *S.S.H. Davarani*, ChemElectroChem. 7, 2816–2825(2020)
10. Y.Y. Chen, Y. Zhang, X. Zhang, T. Tang, H. Luo, S. Niu, Z.H. Dai, L.J. Wan, J.S. Hu, Adv. Mater. **29**, 1703311 (2017)
11. M. Li, J.S. Meng, Q. Li, M. Huang, X. Liu, K.A. Owusu, Z. Liu, L.Q. Mai, Adv. Funct. Mater. **8**, 1802016 (2018)
12. S.Y. Zhou, S. Wang, S.J. Zhou, H.B. Xu, J.P. Zhao, J. Wang, Y. Li, Nanoscale. **12**, 8934–8941 (2020)
13. H.B. Xu, L.T. Gong, S.Y. Zhou, New J. Chem. **44**, 2236–2240 (2020)
14. *A.M. Zardkhoshoui*, *S.S.H. Davarani*, Nanoscale. 12, 1643–1656(2020)
15. *B. Ameri*, *A.M. Zardkhoshoui*, *S.S.H. Davarani*, *Sustain. Energ. Fuels.* 4, 5144–5155(2020)
16. Z.G. Zhang, X. Huang, H.X. Wang, S.H. Teo, T.L. Ma, J. Alloy. Compd. **771**, 274–280 (2019)
17. J.S. Lin, L. Yao, Z.L. Li, P.X. Zhang, W.H. Zhong, Q.H. .Yuan, L.B. Deng, Nanoscale. **11**, 3281–3291 (2019)
18. W.D. He, Z.F. Liang, K.Y. Ji, Q.F. Sun, T.Y. Zhai, X.J. Xu, Nano Res. **11**, 1415–1425 (2018)
19. *A.M. Zardkhoshoui*, *S.S.H. Davarani*, *Chem. Eng. J.* 402, 126241(2020)
20. *A.M. Zardkhoshoui*, *S.S.H. Davarani*, *Nanoscale*, 12, 12(2020)

21. *A.M. Zardkhoshoui*, *M.M. Ashtiani*, *M. Sarparast*, *S.S.H. Davarani*, *J. Power Sources.* 450, 227691(2020)
22. H. Chen, G.H. Jiang, W.J. Yu, D.P. Liu, Y.K. Liu, A.L. Li, Q. Huang, Z.Z. Tong, J. Mater. Chem. A. **4**, 5958–5965 (2016)
23. V. Venkatachalam, A. Alsalme, A. Alswieleh, R. Jayavel, Chem. Eng. J. **321**, 474–483 (2017)
24. S.J. Patil, J. Park, D.W. Lee, In IOP Conference Series: Materials Science and Engineering. **282**, 012004(2017)
25. *B. Liu*, *J. Zhang*, *X.F. Wang*, *G. Chen*, *D. Chen*, *C.W. Zhou*, *G.Z. Shen*, Nano lett. 12, 3005–3011(2012)
26. *X. Wu*, *L. Meng*, *Q. Wang*, *W. Zhang*, *Y. Wang*, *Mater. Lett.* 234, 1–4(2019)
27. Y.P. Huang, Y.E. Miao, H.Y. Lu, T.X. Liu, Chem Eur. J. **21**, 10100–10108**(** (2015) ., **)**
28. Q.H. Wang, Y.X. Zhu, J. Xue, X.S. Zhao, Z.P. Guo, C. Wang, ACS Appl. Mater. Inter. **8**, 17226–17232 (2016)
29. Q.H. Wang, J.L. Du, Y.X. Zhu, J.Q. Yang, J. Chen, C. Wang, L. Li, L.F. Jiao, J. Power Sources. **284**, 138–145 (2015)
30. H. Niu, X. Yang, H. Jiang, D. Zhou, X. Li, T. Zhang, J.Y. Liu, Q. Wang, F.Y. Qu, J. Mater. Chem. A. **3**, 24082–24094 (2015)
31. J.K. Sun, P. Zan, L. Ye, X.J. Yang, L.J. Zhao, J. Mater. Chem. A. **5**, 9815 (2017)
32. H. Wu, Z. Lou, H. Yanga, G.Z. Shen, Nanoscale. **7**, 1921–1926 (2015)
33. S.J. Peng, L.L. Li, H.B. Wu, S. Madhavi, X.W. Lou, Adv. Energy Mater. **5**, 1401172 (2015)
34. M.C. Liu, L.B. Kong, C. Lu, X.J. Ma, X.M. Li, Y.C. Luo, L. Kang, J. Mater. Chem. A. **1**, 1380–1387 (2013)
35. C. Qing, C.X. Yang, M.Y. Chen, W.H. Li, S.Y. Wang, Y.W. Tang, Chem. Eng. J. **354**, 182–190 (2018)
36. Q.H. Wang, L.X. Zhu, L.Q. Sun, Y.C. Liu, L.F. Jiao, J. Mater. Chem. A. **3**, 982–985 (2015)
37. F. Nti, D.A. Anang, J.I. Han, J. Alloy. Compd. **742**, 342–350 (2018)
38. L. Huang, W. Zhang, J.W. Xiang, H.H. Xu, G.L. Li, Y.H. Huang, Sci. Rep. **6**, 31465 (2016)
39. J.L. Sun, S.S. Li, X.R. Han, F. Liao, Y.F. Zhang, L. Gao, H.Y. Chen, C.J. Xu, Ceram. Int. **45**, 12243–12250 (2019)
40. Y.Y. Shang, T. Xie, Y.S. Gai, L.H. Su, L.Y. Gong, H.J. Lv, F.Y. Dong, Electrochim. Acta **253**, 281–290 (2017)
41. X.Z. Li, M.Y. Zhang, L.L. Wu, Q.S. Fu, H. Gao, J. Alloy. Compd. **773**, 367–375 (2019)
42. P. Zhang, J.Y. Zhou, W.J. Chen, Y.Y. Zhao, X.M. Mu, Z.X. Zhang, X.J. Pan, E.Q. Xie, Chem. Eng. J. **307**, 687–695 (2017)
43. P.J. Wang, H.R. Cai, X.L. Li, Y.F. Yang, G. Li, J.L. Xie, H.C. Xia, P.H. Sun, D.S. Zhang, J. Xiong, New J. Chem. **43**, 7065–7073 (2019)
44. W. Qin, J.L. Li, X.Y. Liu, N.F. Zhou, C. Wu, M. Ding, C.K. Jia, J. Colloid Interf. Sci. **554**, 125–132 (2019)
45. D. Cheng, Y.F. Yang, J.L. Xie, C.J. Fang, G.Q. Zhang, J. Xiong, J. Mater. Chem. A. **3**, 14348–14357 (2015)

46. Y.Y. Shang, T. Xie, Y.S. Gai, L.H. Su, L.Y. Gong, H.J. Lv, F.Y. Dong, Electrochim. Acta **253**, 281–290 (2017)

Figures

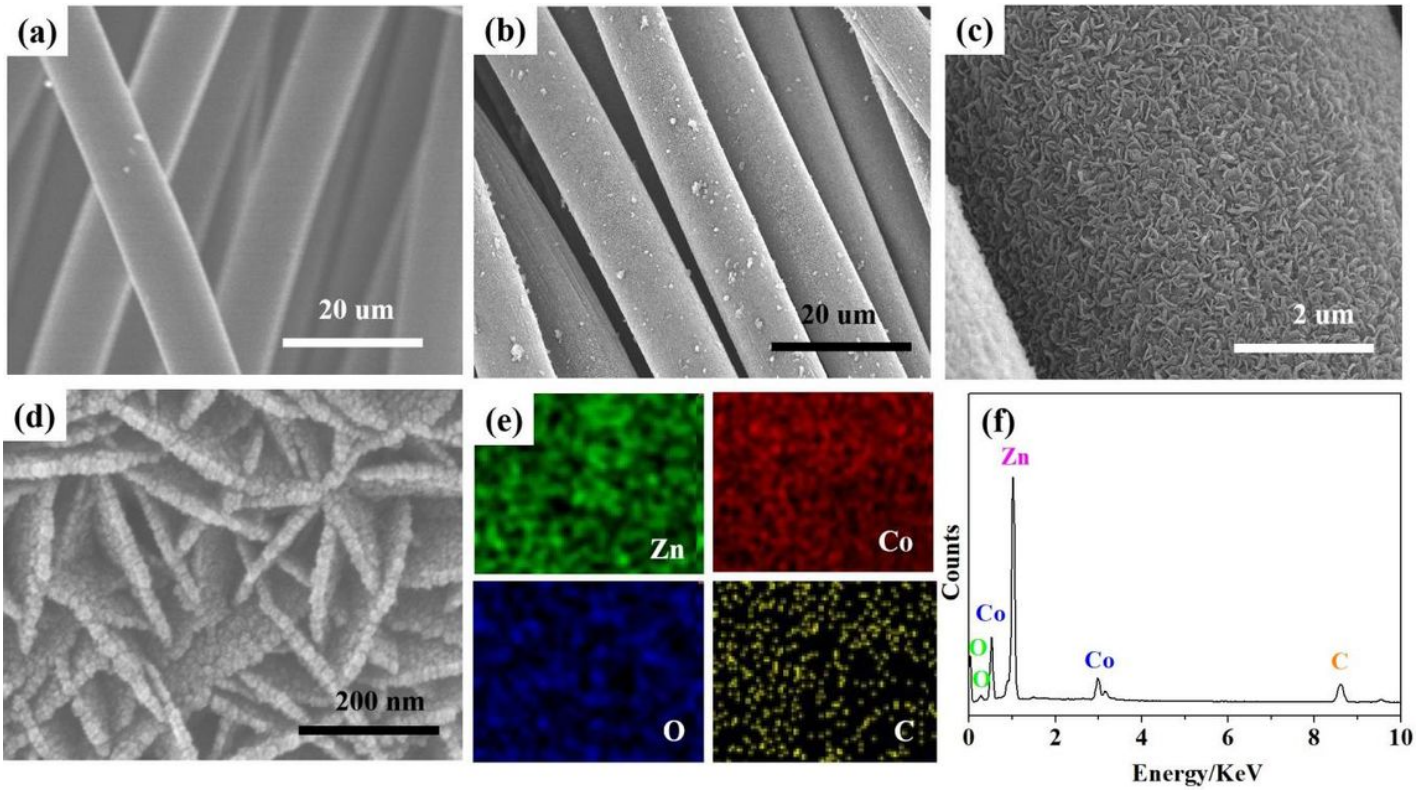

Figure 1

SEM images of carbon cloth (a) and ZnCo2O4 NSs/CC(b-d) at different magnifications; SEM mapping images(e) and EDS spectrum(f) of ZnCo2O4 NSs/CC.

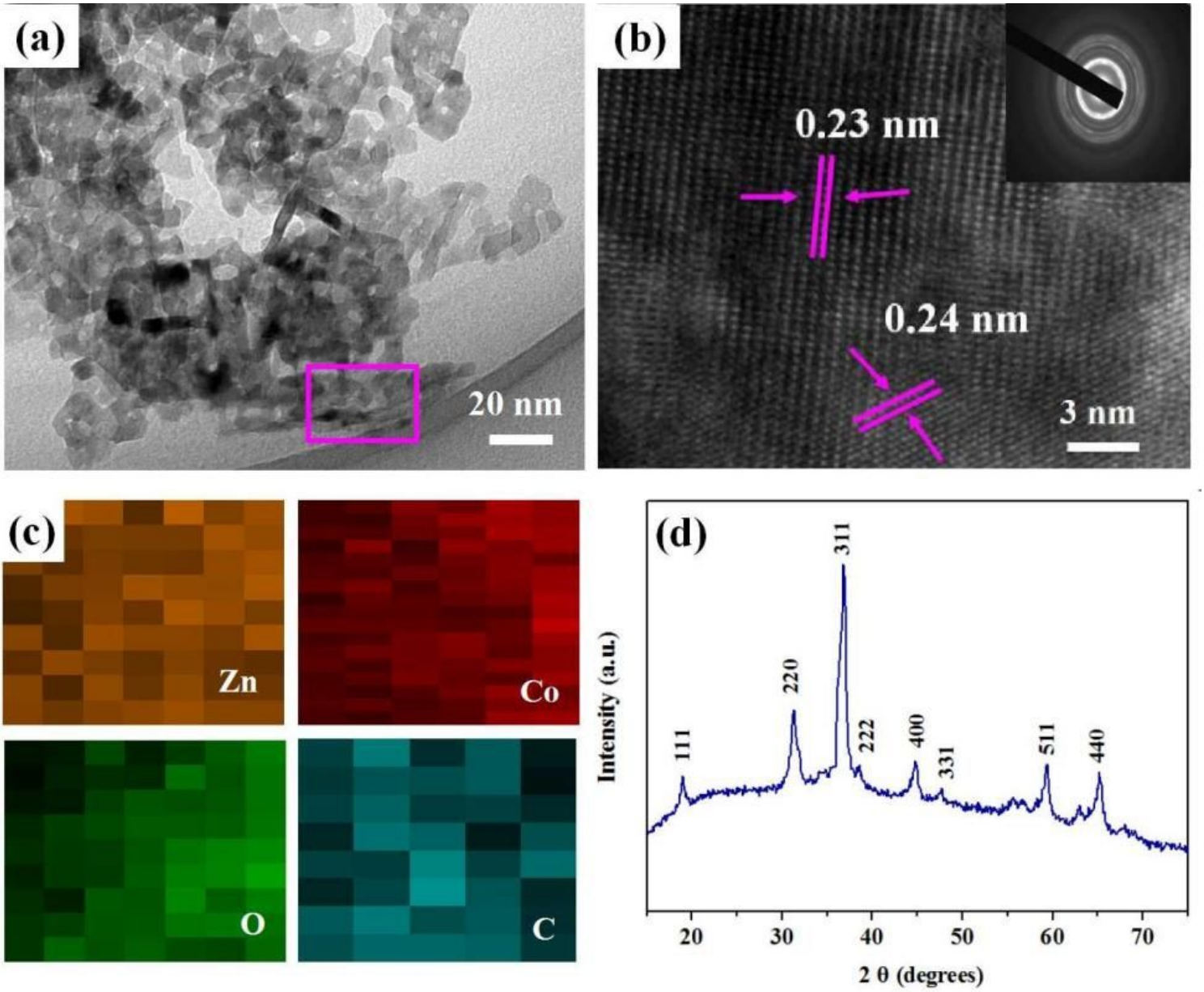

Figure 2

(a) TEM image, (b) HRTEM image of the pink box from (a) and the inset is the corresponding SAED pattern, (c) TEM mapping images of the pink box from (a), and (d) XRD patterns of ZnCo2O4 NSs.

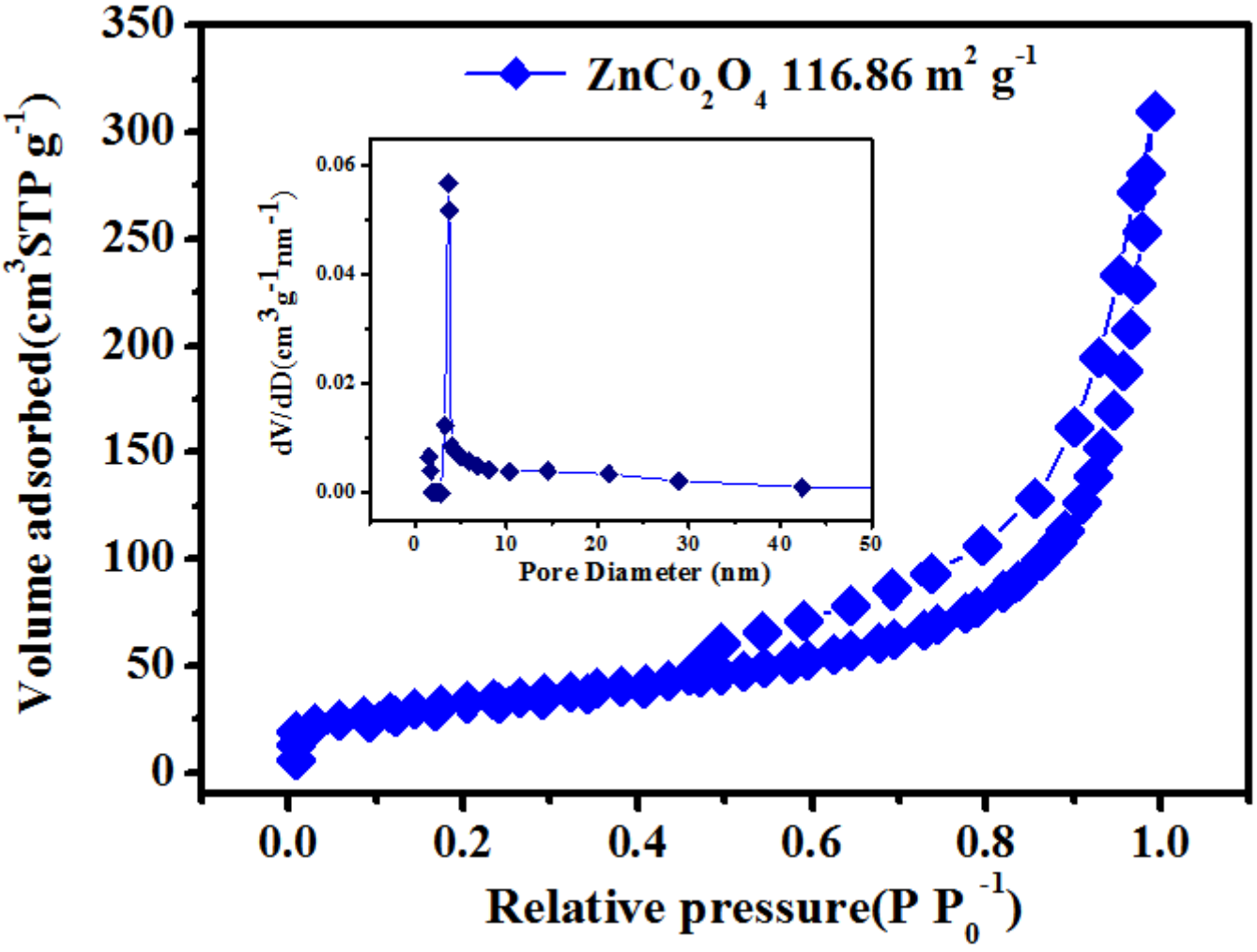

Figure 3

N2 adsorption desorption tests of ZnCo2O4 nanosheets.

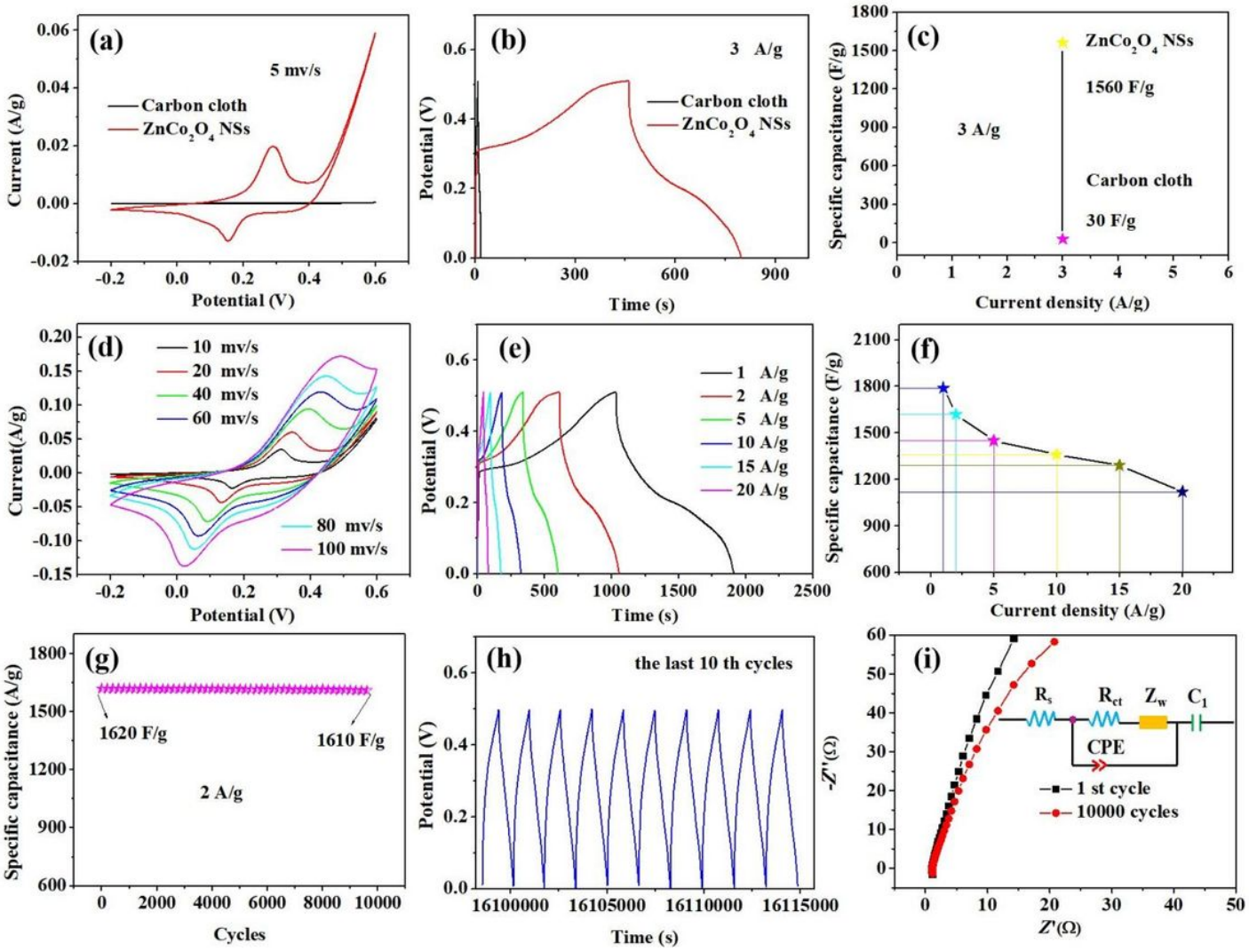

Figure 4

(a) CV curves, (b) Charge-discharge curves, and (c) Specific capacitance of the carbon cloth and ZnCo2O4 NSs/CC; (d) CV curves, (e) Charge-discharge curves, and (f) Specific capacitance of ZnCo2O4 NSs/CC; (g) Cycling performance of ZnCo2O4 NSs/CC at the current density of 2 A g-1; (h) The last 10th cycles of ZnCo2O4 NSs/CC; (i) Nyquist plot of ZnCo2O4 NSs/CC.

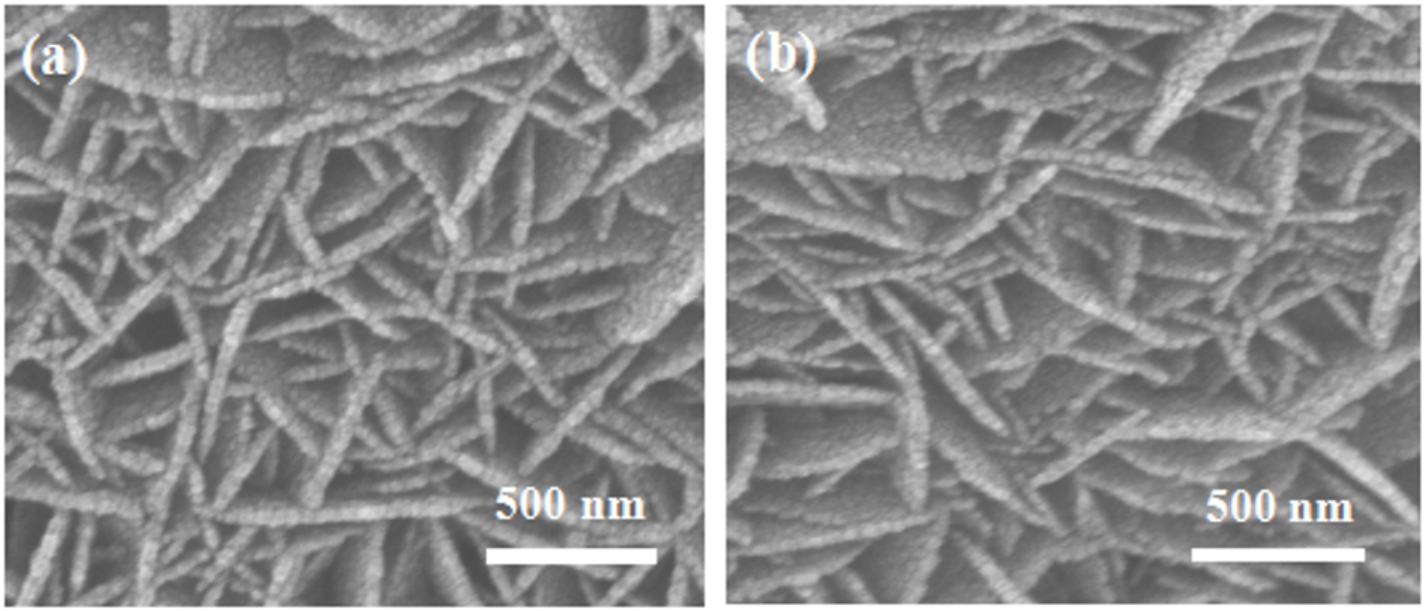

Figure 5

SEM images of the electrode (a) the first cycle (b) after 10000 cycles.

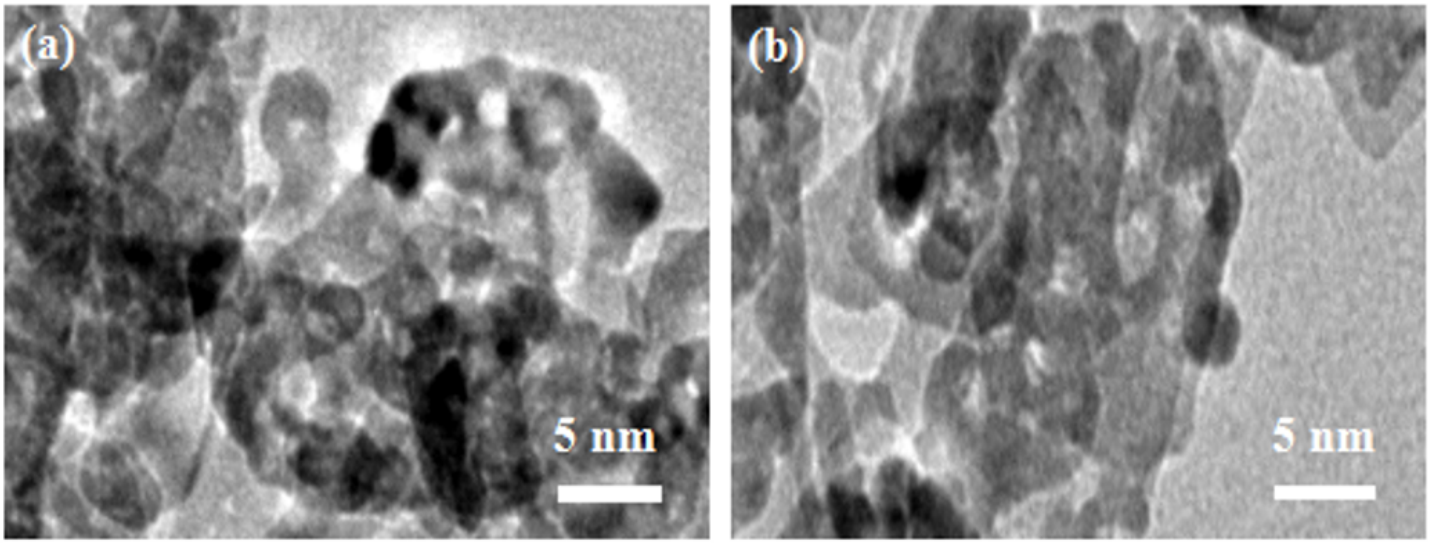

Figure 6

TEM images of the electrode (a) the first cycle (b) after 10000 cycles.

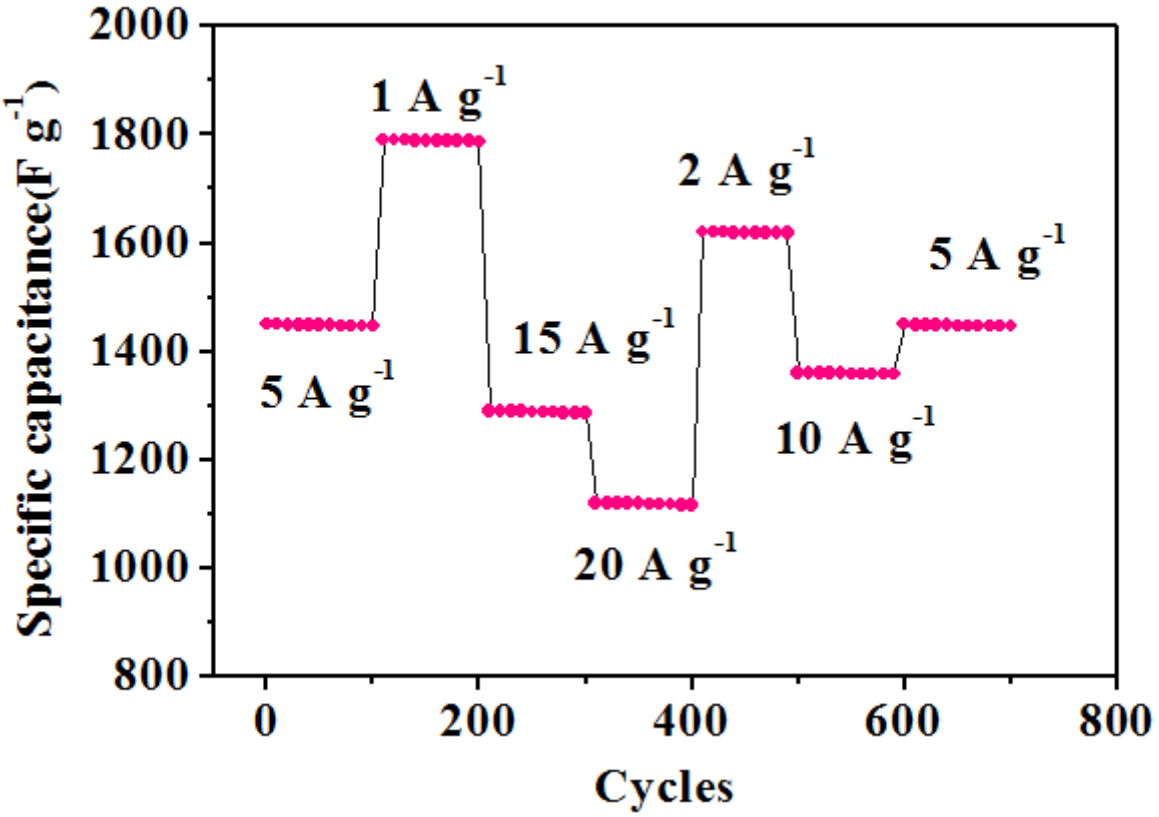

Figure 7

Rate capability and cycle performance of the ZnCo2O4 NAs/CC electrode under different current densities.

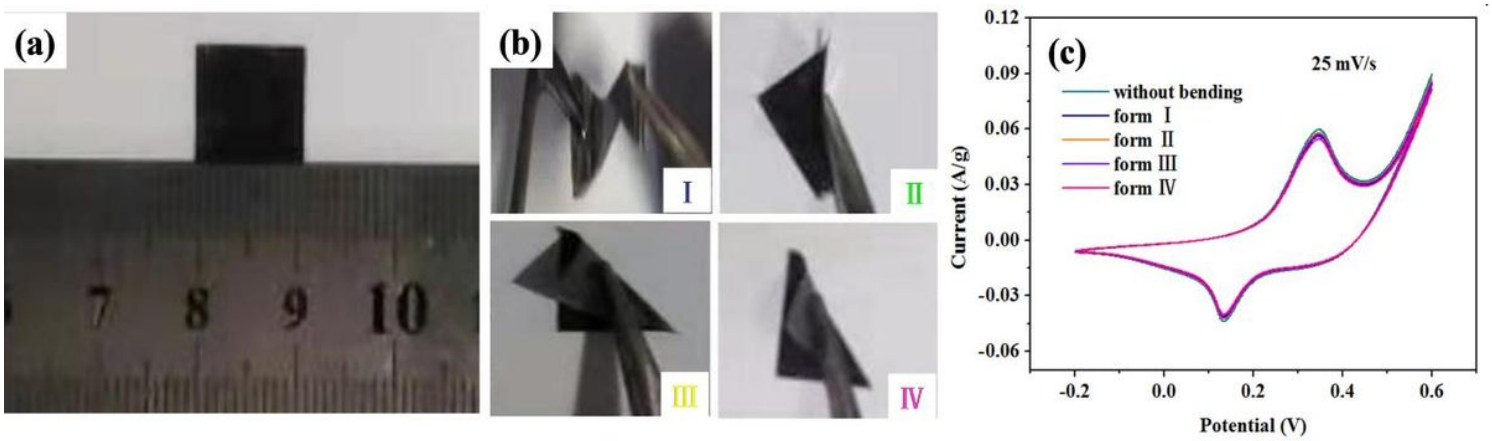

Figure 8

(a)The digital picture of the ZnCo2O4 NSs/CC electrode; (b) ZnCo2O4 NSs/CC electrode undergo four forms by bending and twisting; (c) CV curves of ZnCo2O4 NSs/CC electrode collected at 25 mV/s under different bending conditions.

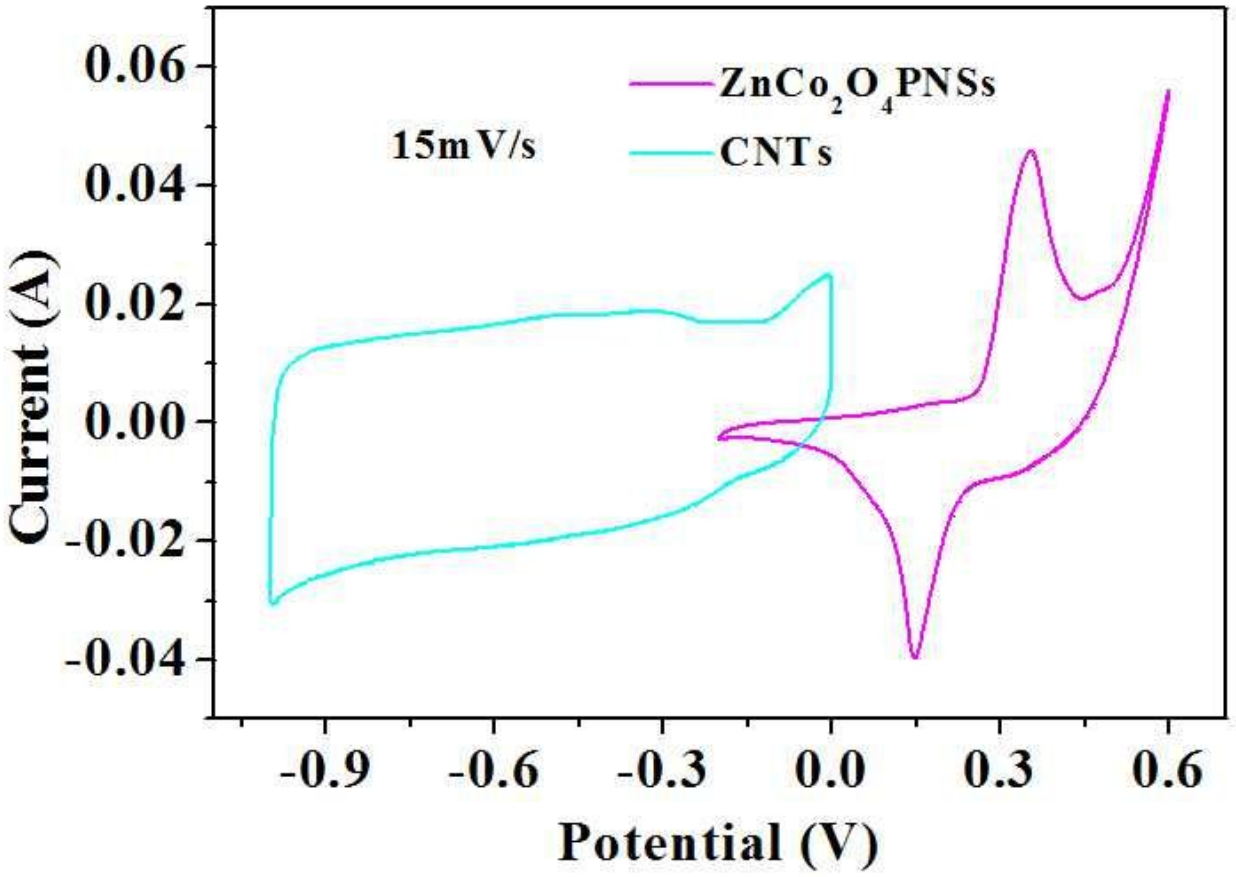

Figure 9

CV curves of the ZnCo2O4 NAs/CC electrode and CNTs/CC electrode in a three-electrode cell at a scan rate of 15 mV/s.

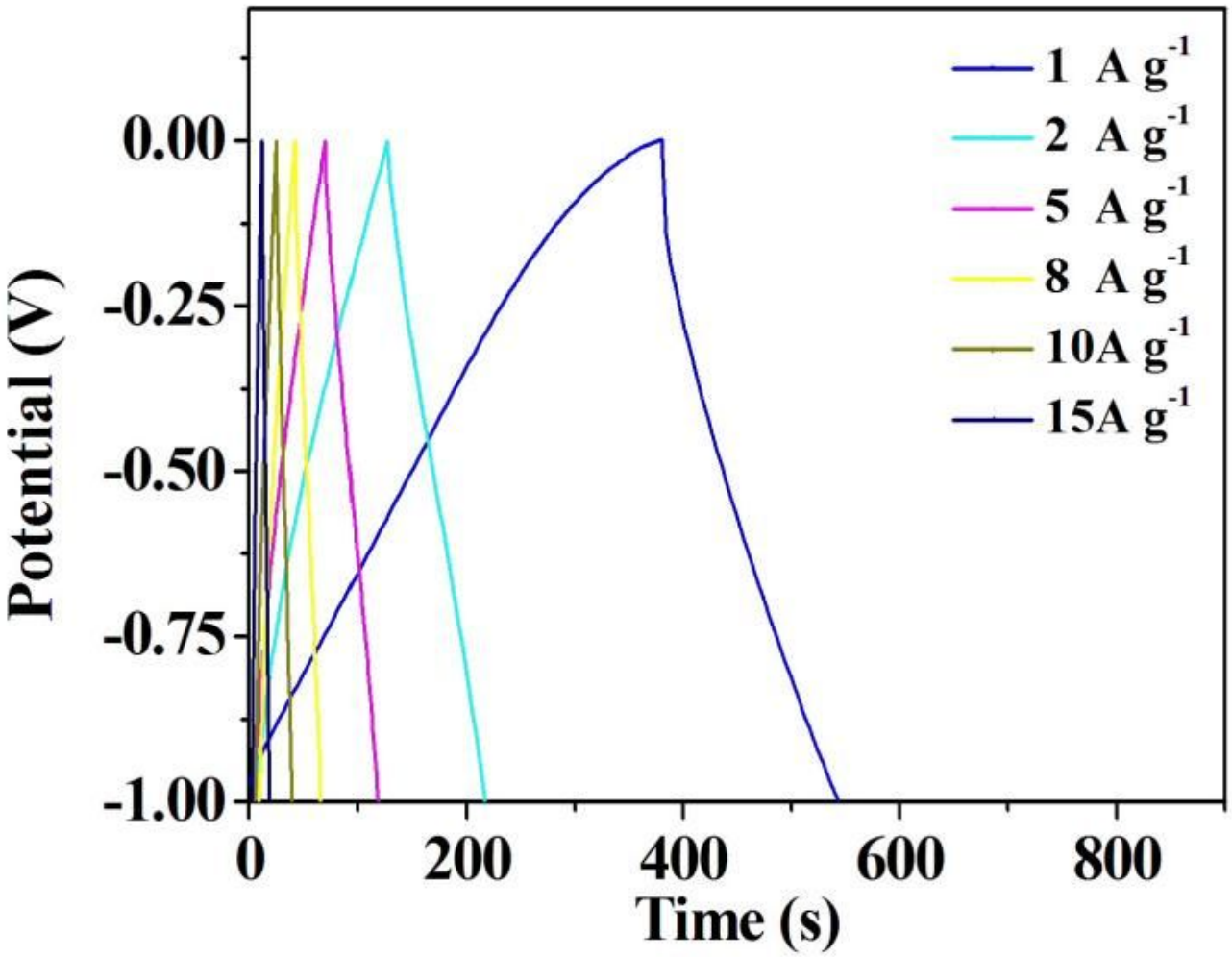

Figure 10

Charge and discharge curves of CNTs at different densities.

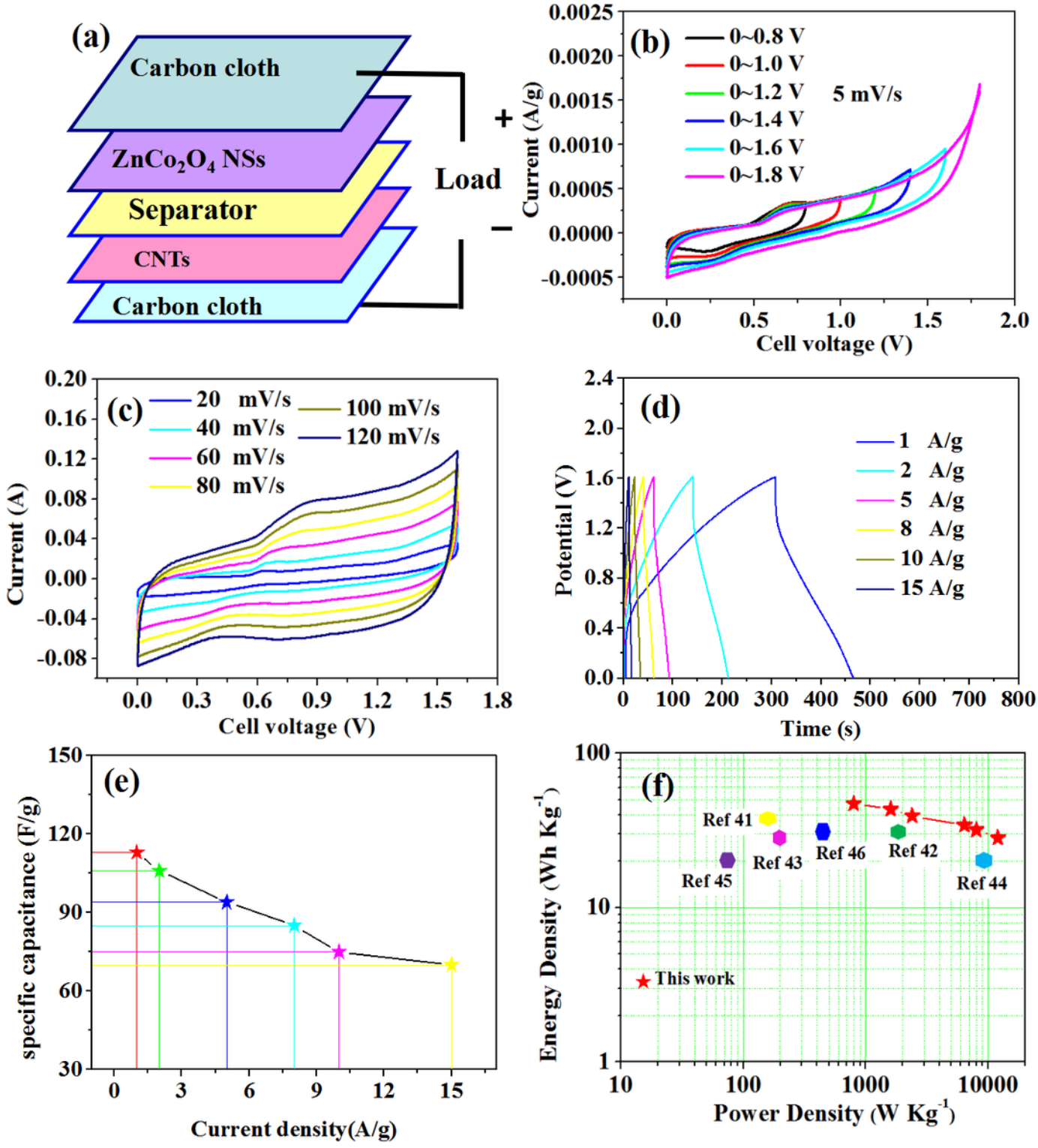

Figure 11

(a) Schematic illustration for the ZnCo2O4 NSs/CC//CNTs/CC ACS device;(b) CV curves of the ACS device at different potential windows; (c) CV curves of the ACS device at different scan rate with potential window 0-1.6 V; (d) Charge-discharge curves of the ACS device at different current densities; (e) Specific capacitance of the ACS device at varied current densities; (f) Ragone plots of the ACS device and other works.